Mikada, H., Moore, G.F., Taira, A., Becker, K., Moore, J.C., and Klaus, A. (Eds.)
Proceedings of the Ocean Drilling Program, Scientific Results Volume 190/196

15. Negative Polarity at the Frontal Thrust—Is Free Gas the Culprit?: Insights from Nankai Accretionary Prism off Cape Muroto Using Seismic-Logging Integration[1]

Sean P.S. Gulick[2] and Nathan L.B. Bangs[2]

ABSTRACT

Within the Nankai accretionary prism off Cape Muroto, Japan, the frontal thrust and thrusts within the imbricate thrust zone show consistent negative polarity fault plane reflections that decrease in amplitude landward. However, the protothrust faults lack a fault plane reflection in three-dimensional seismic data. Differences in velocity and density of the overthrust sections at the proto- and frontal thrusts vs. their underthrust sections is insufficient by an order of magnitude to explain the presence of the fault plane reflection at the frontal thrust. Forward modeling with synthetic seismograms shows that the best match of the logging-while-drilling data with the seismic data at Site 808 is a ~1-m-thick low velocity (1800 m/s) and low density (1.25 g/cm^3) fault zone; however, a wider zone with higher velocity and/or densities is also consistent with the seismic data. High resistivity values across the frontal thrust suggest that the presence of free gas generates the negative polarity reflection. Correlation of the shallowest high-amplitude bright spots along the numerous fault plane reflections from the imbricate thrust zone with the gas hydrate–related bottom-simulating reflector suggests that free gas migrates up the fault zone to pool at the base of the hydrate stability zone and potentially increase concentrations of hydrate above the base of the hydrate stability field. These results suggest that free gas may play a role in generating negative polarity fault plane reflections elsewhere.

[1]Gulick, S.P.S., and Bangs, N.L.B., 2004. Negative polarity at the frontal thrust—is free gas the culprit?: insights from Nankai accretionary prism off Cape Muroto using seismic-logging integration. *In* Mikada, H., Moore, G.F., Taira, A., Becker, K., Moore, J.C., and Klaus, A. (Eds.), *Proc. ODP, Sci. Results,* 190/196, 1–16 [Online]. Available from World Wide Web: <http://www-odp.tamu.edu/publications/190196SR/VOLUME/CHAPTERS/353.PDF>. [Cited YYYY-MM-DD]
[2]Institute for Geophysics, Jackson School of Geosciences, University of Texas, 4412 Spicewood Springs Road, Building 600, Austin TX 78759, USA. Correspondence author: **sean@ig.utexas.edu**

Initial receipt: 1 December 2003
Acceptance: 22 June 2004
Web publication: 20 August 2004
Ms 196SR-353

INTRODUCTION

In May and June of 2001, scientists on Ocean Drilling Program (ODP) Leg 196 investigated the interrelationship between the fluid flow regime and deformation in the Nankai Trough accretionary prism (Fig. F1). During the first part of Leg 196, scientists examined two sites off Cape Muroto, Japan, by drilling with logging-while-drilling (LWD) tools for in situ physical property data (Mikada, Becker, Moore, Klaus, et al., 2002). Leg 196 is part of a larger effort to fully characterize the accretionary processes at the Nankai Trough that includes preceding ODP Legs 131 and 190 (Moore, Taira, Klaus, et al., 2001; Taira, Hill, Firth, et al., 1991), two-dimensional (2-D) and three-dimensional (3-D) seismic reflection and refraction experiments (Aoki et al., 1982, 1986; Bangs et al., 2004; **Bangs and Gulick,** this volume; Gulick et al., 2004; Kodaira et al., 2000; Leggett et al., 1985; Moore et al., 1991; Moore and Shipley, 1993; Moore et al., 1990, 2001; Nasu et al., 1982; Park et al., 1999, 2000; Tamano et al., 1984).

LWD data collected from Site 808 during Leg 196, combined with wireline and core data collected from Site 1174 during Leg 190 (Shipboard Scientific Party, 2001), provide details about fluid expulsion, deformation, diagenesis, and compaction at both the protothrust and frontal thrust zones of the Nankai accretionary prism (Fig. F2). These data are important for the study of accretionary processes on their own, but may prove to be invaluable in that they allow calibration of a 3-D seismic reflection volume that was collected off Cape Muroto in 1999 (Fig. F1) (Gulick et al., 2004; Bangs et al., 2004). Integration of 3-D seismic data with the logging data can greatly extend our understanding of the interplay among deformation, consolidation, and fluid and gas expulsion beyond the one-dimensional (1-D) view provided at individual drill sites.

Within the protothrust and imbricate thrust zones of the Nankai Trough accretionary prism, the existence, polarity, and strength of fault plane reflections vary substantially in 3-D (Fig. F3). In general, the protothrust faults are recognized from offsets in the Shikoku Basin strata and not as fault plane reflections, whereas the thrusts within the imbricate thrust zone display negative polarity fault plane reflections (e.g., Gulick et al., 2004) (Fig. F3). Leg 196 Hole 808I penetrated through the frontal thrust using LWD technology, whereas Leg 190 Hole 1174B cored through the protothrust. The Leg 190 cores were subsequently logged onboard the *JOIDES Resolution*. In this paper, we compare the velocity and density data from Sites 808 and 1174 to demonstrate that the presence of a negative polarity fault plane reflection at the frontal thrust, but not at the protothrust, is due to differences in the physical properties within the fault zones. We show evidence from the logging data for a distinct velocity and density drop at the frontal thrust at Site 808 and model the frontal thrust reflection in 1-D in Hole 808I. Our results suggest fluid-transported free gas may play an important role in generating the negative polarity fault plane reflection at Site 808. Using this information, we examine the pattern and discuss the implications of the negative polarity fault plane reflections present throughout the imbricate thrust zone.

F1. Study area, p. 11.

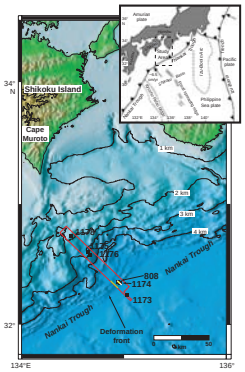

F2. Protothrust vs. frontal thrust, p. 12.

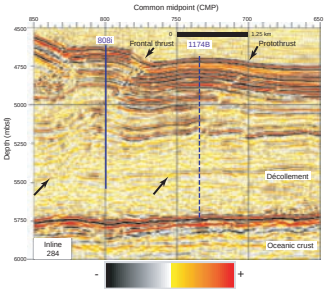

F3. 3-D and 2-D views of imbricate thrust zone, p. 13.

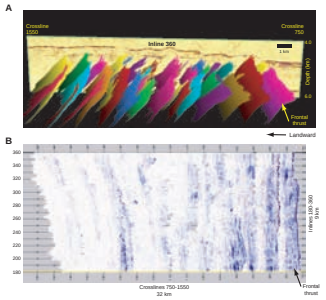

METHODS

The results presented in this paper use several different data sets: the time-migrated, depth-converted Muroto 3-D seismic volume described in Gulick et al. (2004), the Site 808 LWD ISONIC velocities processed by **Goldberg et al.** (this volume), filtered Site 808 LWD densities, and the core-derived velocities and densities from Hole 1174B (Shipboard Scientific Party, 2001). J.C. Moore (University of California, Santa Cruz, California, USA) filtered the Site 808 LWD densities by removing suspect density values, where the differential caliper is >1 in and the time-at-bit (TAB) is >1.5 hr. For integration of the logging data with the seismic data, we built synthetic seismograms using Schlumberger's Geoframe system and then modeled selected possible impedances within the frontal thrust in an effort to determine the origin of the negative polarity fault zone. During the forward modeling, we scaled the synthetic seismograms to best match the reflection amplitude at the seafloor and then compared the waveform and amplitude of the synthetic at the frontal thrust. For our 1-D modeling presented in this paper, we scaled the LWD ISONIC velocity values up by 12.5%, as **Goldberg et al.** (this volume) showed that the ISONIC velocities at Site 808I underestimate velocity by 12.5% on average. We extrapolated the modeling results throughout the imbricate thrust zone by extracting the amplitudes of the fault plane reflections on migrated data, corrected only for spherical divergence.

RESULTS

Theoretically, negative polarity fault plane reflections can be generated by inherent physical properties of the fault zone or by contrasts in velocity and density in the rocks above and below the fault zone. In the latter case, a more dewatered hanging wall thrust over a less dewatered and less compacted footwall could result in sufficient contrast in acoustic impedance to produce the observed negative polarity reflection. The presence of a negative polarity fault plane reflection at Site 808 and the lack of one at Site 1174 (Fig. **F2**) provides an excellent opportunity to examine the physical properties that need to be present to observe a fault plane reflection.

To differentiate between the potential causes, we calculated the average velocity and density for 10 m above and below the protothrust and frontal thrust faults (see Fig. **F4A, F4B**) to examine the differences in physical properties in the hanging wall and footwall. We determined the reflection coefficient, R, for each surface using a simplified version of Zoeppritz's equation, which assumes vertical incidence:

$$R = (v_2\rho_2 - v_1\rho_1)/(v_2\rho_2 + v_1\rho_1),$$

where v_1 and v_2 and ρ_1 and ρ_2 are the velocities and densities of the two layers, respectively. The average LWD-determined velocity and density in the 10 m of the hanging wall above the frontal thrust are 1917 m/s and 2.07 g/cm³, respectively, and those in the 10 m of the footwall below the frontal thrust are 1923 m/s and 2.05 g/cm³, respectively. The resulting reflection coefficient, R, is –0.0038. In contrast, R for the protothrust at Site 1174 is –0.0004, using 10-m average core-derived values above and below protothrust of 1950 m/s and 2.07 g/cm³, respectively, and 1939 m/s and 2.08 g/cm³, respectively.

F4. Velocity, density, and synthetic seismograms, p. 14.

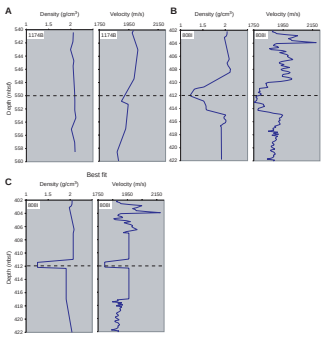

To put these values in perspective, the reflection coefficient at the seafloor at Site 808 is ~0.2. The measured acoustic amplitude for the seafloor reflection at Site 808I is 94,576, whereas the measured acoustic amplitude of the frontal thrust reflection at Site 808I is –17,789. Assuming the ratios are proportional based on magnitude, the reflection coefficient necessary to explain the negative polarity fault plane reflection at the frontal thrust should be approximately –0.0376, which is an order of magnitude larger than the hanging wall over footwall physical properties contrast alone could produce. Therefore the negative polarity frontal thrust reflection must be generated by the physical properties inherent to the fault zone itself. In contrast, the lack of a reflection at the protothrust fault suggests the only physical property effects generating reflectivity in Hole 1174B are the contrasts in the hanging wall vs. footwall, which at –0.0004 are too small to produce a reflection.

For the frontal thrust, the alternative possibility—the one favored in the majority of accretionary prism studies (e.g., Moore et al., 1995; Bangs et al., 1999)—is that the negative polarity reflection stems from a thin-bed phenomenon, where the fault zone itself is substantially lower in velocity and density than the rocks of the hanging wall or footwall. For instance, dilation of the fault zone by channelized pore fluids produced in prism dewatering could reduce the velocity and density within the frontal thrust. An examination of the Leg 196 Site 808 LWD data partly supports this concept, as there is a marked density low at the frontal thrust and some evidence for lower velocities as well (Fig. **F4B**). The lack of either low velocity or density data across the protothrust (Fig. **F4A**) is consistent with the fault in Hole 1174B simply being the glide plane between the hanging wall and footwall, and not having developed into a fault zone.

The width of the low density values from the filtered LWD data in Hole 808I is ~4 m (410.71–414.22 meters below seafloor [mbsf]), with the lowest values located at ~412 mbsf across a zone 0.2–1 m wide. Correspondingly, low velocity values lie over a ~4.5-m-thick zone (409.9–414.5 mbsf); the lowest values are located at ~412 mbsf across a ~2.1-m zone (Fig. **F4B**). To test if a 4–4.5 m low velocity and density fault zone would produce the observed reflectivity in the 3-D data, we produced a synthetic seismogram built using the LWD velocity and density data at the frontal thrust. The resulting synthetic seismogram has much greater amplitude than the acquired data (Fig. **F4D**).

The fact that the 4–4.5-m fault zone observed in the LWD data generates reflectivity greater than that observed in the Muroto 3-D volume at Site 808I is problematic. In order to decrease the amplitude of the reflectivity, the fault zone must either be of similar thickness but higher velocity and/or density or the fault zone must be thinner.

In order to evaluate the necessary thickness of the fault zone to best match the acquired seismic data, we ran a series of 1-D forward models. The best-fit model (Fig. **F4C**) consists of a low velocity (1795 m/s) and density (1.26 g/cm^3) layer ~1 m thick, similar to the thickness of the low density center of the fault observed in the LWD density data (Fig. **F4B**) but with more rapid transitions into the hanging wall and footwall properties. The values of this thin low velocity and density zone are consistent with the lowest recorded values within fault zone by the LWD tools. This thin-bed model produces a synthetic seismogram of similar waveform and amplitude to the acquired data (Fig. **F4E**).

DISCUSSION

Accretion of high-porosity, fluid-enriched sediments at convergent margins results in porosity loss and dewatering (Moore and Vrolijk, 1992; Moore et al., 1991; Bray and Karig, 1985). Negative polarity of fault zone reflections in seismic images of accretionary prism faults have commonly been interpreted as being caused by overpressured fluids that are channelized within the fault zones (e.g., Moore et al., 1995; Bangs et al., 1999). Theoretically, however, negative polarity fault plane reflections can be generated by more consolidated and dewatered sediments being thrust over less consolidated sediments across the fault. We demonstrate above that the difference in physical properties of the hanging wall vs. footwall is insufficient to create the negative polarity reflection observed at Site 808.

The LWD data at Hole 808I implies the frontal thrust is a ~4-m-thick fault zone with peak low velocities at ~1775 m/s and densities at ~1.25 g/cm^3. However, our modeling results show that velocities and densities this low over ~4 m would create a greater negative polarity fault plane reflection than is observed. Our modeling suggests the negative polarity reflection from the frontal thrust at Site 808 could be generated by a 1-m-thick low velocity and low density zone centered at ~412 mbsf (Fig. **F4C**) or by a ~4-m-thick fault zone with higher velocities and/or densities than recorded.

Explanations for this mismatch in the observations of the seismic and LWD data include potential interference effects reducing the acquired reflectivity of the fault plane in the seismic data, poor spatial collocation of the modeled portion of the 3-D seismic data and the borehole due to navigation errors or a deviated borehole, or underestimation of the velocity and/or density at the fault zone by the LWD tools. **Goldberg et al.** (this volume) demonstrate that the LWD ISONIC velocity data on average underestimates the velocity by 12.5% based on ties with the 3-D seismic data. For building the 1-D forward models, we uniformly increased the velocities by 12.5% to account for this known underestimation. This correction assumes the underestimation by the LWD ISONIC tool is the same at all depths in the borehole; however, conditions in the borehole at the frontal thrust (larger caliper values and evidence of overpressuring in the form of borehole breakouts surrounding the fault zone) may yield less accurate estimations of velocity or, potentially, density. Interestingly, the LWD density data suggests a low-density center to the fault zone (Fig. **F4B**) consistent with the thin-bed model (Fig. **F4C**). We suggest it is currently inconclusive as to what the exact physical description of the frontal thrust fault zone is with possible endmembers being a 1-m-thick low velocity/density zone as modeled here or a 4-m-thick zone with higher velocities and/or densities than the 1m thick case but lower than the hanging wall and footwall. In the latter case the velocities and/or densities need to be higher in the fault zone than those recorded by the LWD tools.

Resistivity results from Leg 196 LWD at Site 808 show a pronounced spike in the resistivity at the frontal thrust (Mikada, Becker, Moore, Klaus, et al., 2002). This spike in resistivity was interpreted to stem from a compacted fault zone (Shipboard Scientific Party, 2002). This interpretation is inconsistent with both the velocity and density data and with our seismic modeling results. We suggest instead that the resistivity is not caused by compaction in the fault zone but rather a small percentage of free gas within the pore space, potentially along the 1-m-thick center of the fault, and that this small amount of free gas is the primary

cause for the fault plane reflection at the frontal thrust. By extension, it is possible that the negative polarity fault plane reflections are either caused or enhanced by varying amounts of free gas in the fault zones throughout the remainder of the imbricate thrust zone (Fig. F3).

Evidence for a relationship between the faulting and the upward advection of free gas throughout the imbricate thrust zone lies in the strong correlation between the cessation of the high-amplitude fault-plane reflections and the bottom-simulating reflector (BSR) within the 3-D volume (e.g., Fig. F5). On continental margins throughout the world, BSRs are present at the top of a layer of free gas that is dynamically maintained by the advection of gas from sediments below and the conversion of the free gas into gas hydrates above (e.g., Shipley et al., 1979; MacKay et al., 1994). Studies of BSRs have sometimes noted perturbations in the reflectivity of the BSR in the vicinity of a fault that has generally been interpreted as either a thermal or salinity effect caused by advecting fluids (e.g. Rowe and Gettrust, 1993; Taylor et al., 2000). Our observation that the imbricate thrust faults at Nankai frequently cease to be negative in polarity at the depth of the BSR suggests that free gas being advected with the fluids in the fault zones in part feeds the hydrate system from beneath. Similarly, Rowe and Gettrust (1993) suggested that, for Blake Ridge, the presence of faults allowed free gas from beneath the base of gas hydrate stability to migrate into this zone and be converted into hydrate in the overlying sediments. We suggest the flux of free gas through the frontal thrust into the hydrate stability zone results in a reduction of free gas in the fault itself, likely due in part to decreasing solubility with depth, and a loss of negative polarity. It is possible that this process would result in greater concentrations of hydrate within sediments above the base of the hydrate stability zone that are near the imbricate thrusts relative to those farther away. Based on the 3-D images, the BSR brightens (high-amplitude negative polarity reflections) above the hanging-wall thrusts and on the footwall side of the thrusts, as can be seen in Figure F5. We suggest this increased reflectivity of the BSR is due to free gas preferentially being fed to the base of the hydrate system by the imbricate thrusts. Increases in reflectivity of a BSR near faulting have also been noted for normal faults on Blake Ridge (Taylor et al., 2000) and thrust faults on the South Shetland Margin (Lodolo et al., 2002).

The thickness of the high-resistivity zone across the frontal thrust is wider (Mikada, Becker, Moore, Klaus, et al., 2002) than the modeled 1-m fault discussed here, suggesting that if the free gas-transporting permeable portion of the fault is indeed only 1 m thick then the free gas may leak upwards into the overlying deformed zone above the fault (J.C. Moore, pers. comm.). This diffusion must be slow enough relative to the advection along the fault that the concentrations in the permeable portion of the fault remain high enough to generate a reflection and low enough in the overlying material to not generate one. Alternatively the thicker resistivity spike might lend support to a wider free-gas bearing fault zone.

One argument against free gas in the fault zones off Muroto is that the cores from Site 808 did not show any anomalous headspace gas (Shipboard Scientific Party, 1991). However, BSRs have been drilled in many locations (e.g. Suess, von Huene, et al., 1988; Shipboard Scientific Party, 1994; Shipboard Scientific Party, 2001), and only in cases where the free gas in unusually high has it been detected in the head space (e.g. Tréhu, Bohrmann, Rack, Torres, et al., 2003). Additionally, core recovery at Site 808 across the frontal thrust was low (Shipboard Scientific

F5. Reflectivity and BSRs, p. 16.

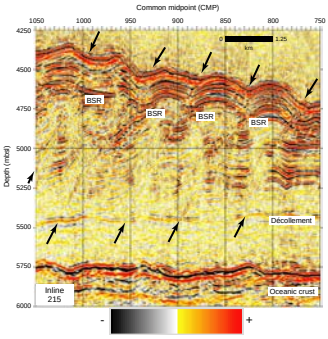

Party, 1991) and the area of highest gas concentration may not have been adequately sampled.

Free gas within the fault zones may not be the only contributor to negative polarity fault plane reflections, as there are some examples of reflections from fault segments close to the décollement where gas solubility would be high (e.g., common depth point 900, Fig. F5). However, for the majority of the imaged fault plane reflections in the 3-D volume the correspondence of bright reflections from the regions below the hydrate stability field, as marked by the BSR, and the cessation above suggest free gas is the dominant effect on the fault plane reflectivity (Fig. F5). The frontal thrust itself is an exception that may be due to the base of the gas hydrate stability zone being close to the seafloor (Fig. F5); alternatively, in the case of the frontal thrust and the few other thrusts where the negative polarity reflections continue past the BSR, we might conclude the advective flow is high enough at those faults to allow the free gas to persist en route to the seafloor.

Figure F3 shows the amplitude of the fault plane reflections for each of the thrust faults within the imbricate thrust zone (all thrusts between the frontal thrust and the first out-of-sequence thrust). The amplitudes of the fault plane reflections are largely negative (although there are isolated positive polarity reflections) throughout the imbricate thrust zone; however, the amplitudes become less negative landward. The presence of the isolated positive polarity segments along some of the faults interpreted with our free-gas hypothesis in mind might suggest that in any given moment in time (such as the "snapshot" represented by the Muroto 3-D data) there will be segments of the imbricate thrust faults not currently containing the necessary free gas. It is possible that these systems are highly variable in reflectivity on the timescale of gas migration and would be worth testing in future studies. Regionally, the lessening of the negative amplitudes landward is greatest upslope of the fourth and fifth thrusts, where the faults generate reduced topographic expression and therefore may be less active (Gulick et al., 2004). Given the evidence presented above, this lessening may be related to a reduction in the fluid-transported free gas.

Our interpretation of these observations is that the thrust faults in the imbricate thrust zone have progressively less gas within the faults in the landward direction and, by extension, less dewatering occurring along the more landward faults. We suggest this trend is due to two factors: (1) the amount of dewatering required of the sediments during accretion decreases landward, and (2) the fault zones themselves are less active and therefore are less efficient conduits of fluid. Active fault zones deform frequently within the earthquake cycle and thus continue to generate porosity via the generation of breccia and fault gouge, whereas less active faults may lose this porosity due to mineralization and compaction (e.g., Jarrard, 1997).

CONCLUSIONS

The negative polarity fault plane reflection at Site 808 is caused by a physical property change inherent to the fault zone. Our best-fit model using synthetic seismograms to test differing physical natures of the fault zone is a 1-m-thick low velocity and low density zone at ~412 mbsf; however, a wider fault zone with higher velocities and/or densities is also possible. Based on a resistivity spike and a strong correlation with the cessation of negative polarity reflections and the BSR, we pro-

pose the negative polarity reflection is generated by a few percent free gas. The remaining thrusts of the imbricate thrust zone also exhibit negative polarity fault plane reflections that brighten upward and, in most cases, cease at the BSR. The regional pattern of the fault plane reflections from the 3-D volume shows a landward decrease in amplitudes of the fault plane reflections. This decrease in negative amplitudes may be due to less dewatering of the prism and/or the fault zones becoming less efficient pathways.

ACKNOWLEDGMENTS

We thank the captain, crew, and technicians of the *JOIDES Resolution*. This research used data provided by the Ocean Drilling Program (ODP). ODP is sponsored by the U.S. National Science Foundation (NSF) and participating countries under the management of Joint Oceanographic Institutions (JOI), Inc. Funding for this research was provided by the U.S. Science Support Program. This paper is UTIG contribution number 1691.

REFERENCES

Aoki, Y., Kinoshita, H., and Kagami, H., 1986. Evidence of a low-velocity layer beneath the accretionary prism of the Nankai Trough; inference from a synthetic sonic log. *In* Kagami, H., Karig, D.E., Coulbourn, W.T., et al., *Init. Repts. DSDP,* 87: Washington (U.S. Govt. Printing Office), 727–735.

Aoki, Y., Tamano, T., and Kato, S., 1982. Detailed structure of the Nankai Trough from migrated seismic sections. *In* Watkins, J.S., and Drake, C.L. (Eds.), *Studies in Continental Margin Geology.* AAPG Mem., 34:309–322.

Bangs, N.L.B., Shipley, T.H., Gulick, S.P.S., Moore, G.F., Kuromoto, S., and Nakamura, Y., 2004. Evolution of the Nankai Trough décollement from the trench into the seismogenic zone: inferences from three-dimensional seismic reflection imaging. *Geology,* 32:273–276.

Bangs, N.L., Shipley, T.H., Moore, J.C., and Moore, G., 1999. Fluid accumulations and channeling along the Northern Barbados Ridge décollement thrust. *J. Geophys. Res.,* 104:20399–20414.

Bray, C.J., and Karig, D.E., 1985. Porosity of sediments in accretionary prisms and some implications for dewatering processes. *J. Geophys. Res.,* 90:768–778.

Gulick, S.P.S., Bangs, N.L.B., Shipley, T.H., Nakamura, Y., Moore, G., and Kuramoto, S., 2004. Three-dimensional architecture of the Nankai accretionary prism's imbricate thrust zone off Cape Muroto, Japan: prism reconstruction via en echelon thrust propagation. *J. Geophys. Res.,* 109:10.1029/2003JB002654.

Jarrard, R.D., 1997. Origins of porosity and velocity variations at Cascadia accretionary prism. *Geophys. Res. Lett.,* 24:325–328.

Kodaira, S., Takahashi, N., Park, J., Mochizuki, K., Shinohara, M., and Kimura, S., 2000. Western Nankai Trough seismogenic zone: results from a wide-angle ocean bottom seismic survey. *J. Geophys. Res.,* 105:5887–5905.

Leggett, J.K., Aoki, Y., and Toba, T., 1985. Transition from frontal accretion to underplating in a part of the Nankai Trough accretionary complex off Shikoku (SW Japan) and extensional features on the lower trench slope. *Mar. Pet. Geol.,* 2:131–141.

Lodolo, E., Camerlenghi, A., Madrussani, G., Tinivella, U.,and Rossi, G., 2002. Assessment of gas hydrate and free gas distribution on the South Shetland margin (Antarctica) based on multichannel seismic reflection data. *Geophys. J. Int.,* 148:103–119.

MacKay, M.E., Jarrard, R.D., Westbrook, G.K., and Hyndman, R.D., 1994. Origin of bottom-simulating reflectors: geophysical evidence from the Cascadia accretionary prism. *Geology,* 22:459–462.

Mikada, H., Becker, K., Moore, J.C., Klaus, A., et al., 2002. *Proc. ODP, Init. Repts.,* 196 [CD-ROM]. Available from: Ocean Drilling Program, Texas A&M University, College Station TX 77845-9547, USA.

Moore, G.F., and Shipley, T.H., 1993. Character of the décollement in the Leg 131 area, Nankai Trough. *In* Hill, I.A., Taira, A., Firth, J.V., et al., *Proc. ODP, Sci. Results,* 131: College Station, TX (Ocean Drilling Program), 73–82.

Moore, G.F., Shipley, T.H., Stoffa, P.L., Karig, D.E., Taira, A., Kuramoto, S., Tokuyama, H., and Suyehiro, K., 1990. Structure of the Nankai Trough accretionary zone from multichannel seismic reflection data. *J. Geophys. Res.,* 95:8753–8765.

Moore, G.F., Taira, A., Bangs, N.L., Kuramoto, S., Shipley, T.H., Alex, C.M., Gulick, S.S., Hills, D.J., Ike, T., Ito, S., Leslie, S.C., McCutcheon, A.J., Mochizuki, K., Morita, S., Nakamura, Y., Park, J.O., Taylor, B.L., Toyama, G., Yagi, H., and Zhao, Z., 2001. Data report: Structural setting of the Leg 190 Muroto transect. *In* Moore, G.F., Taira, A., Klaus, A., et al., *Proc. ODP, Init. Repts.,* 190, 1–14 [CD-ROM]. Available from: Ocean Drilling Program, Texas A&M University, College Station TX 77845-9547, USA.

Moore, G.F., Taira, A., Klaus, A., et al. 2001. *Proc. ODP, Init. Repts.,* 190 [CD-ROM]. Available from: Ocean Drilling Program, Texas A&M University, College Station TX 77845-9547, USA.

Moore, J.C., Brown, K.M., Horath, F., Cochrane, G., MacKay, M., and Moore, G., 1991. Plumbing accretionary prisms: effects of permeability variations. *Philos. Trans. R. Soc. London, Ser. A,* 335:275–288.

Moore, J.C., Moore, G.F., Cochrane, G.R., and Tobin, H.J., 1995. Negative-polarity seismic reflections along faults of the Oregon accretionary prism: indicators of overpressuring. *J. Geophys. Res.,* 100:12895–12906.

Moore, J.C., and Vrolijk, P., 1992. Fluids in accretionary prisms. *Rev. Geophys.,* 30:113–135.

Nasu, N., et al., 1982. Multi-channel seismic reflection data across Nankai Trough. In *IPOD-Japan Basic Data Ser.:* Tokyo (Ocean Res. Inst.), 4:34.

Park, J.-O., Tsuru, T., Kaneda, Y., Kono, Y., Kodaira, S., Takahashi, N., and Kinoshita, H., 1999. A subducting seamount beneath the Nankai accretionary prism off Shikoku, southwestern Japan. *Geophys. Res. Lett.,* 26:931–934.

Park, J.-O., Tsuru, T., Kodaira, S., Nakanishi, A., Miura, S., Kaneda, Y., Kono, Y., and Takahashi, N., 2000. Out-of-sequence thrust faults developed in the coseismic slip zone of the 1946 Nankai earthquake (Mw = 8.2) off Shikoku, southwest Japan. *Geophys. Res. Lett.,* 27:1033–1036.

Rowe, M.M., and Gettrust, J.F., 1993. Faulted structure of the bottom-simulating reflector on the Blake Ridge, western North Atlantic. *Geology,* 21:833–836.

Shipboard Scientific Party, 1991. Site 808. *In* Taira, A., Hill, I., Firth, J.V., et al., *Proc. ODP, Init. Repts.,* 131: College Station, TX (Ocean Drilling Program), 71–269.

Shipboard Scientific Party, 1994. Site 888. *In* Westbrook, G.K., Carson, B., Musgrave, R.J., et al., *Proc. ODP, Init. Repts.,* 146 (Pt. 1): College Station, TX (Ocean Drilling Program), 55–125.

Shipboard Scientific Party, 2001. Site 1174. *In* Moore, G., Taira, A., Klaus, A., et al., *Proc. ODP, Init. Repts.,* 190, 1–149 [CD-ROM]. Available from: Ocean Drilling Program, Texas A&M University, College Station TX 77845-9547, USA.

Shipboard Scientific Party, 2002. Site 808. *In* Mikada, H., Becker, K., Moore, J.C., Klaus, A., et al., *Proc. ODP, Init. Repts.,* 196, 1–68 [CD-ROM]. Available from: Ocean Drilling Program, Texas A&M University, College Station TX 77845-9547, USA.

Shipley, T.H., Houston, M.H., Buffler, R.T., Shaub, F.J., McMillen, K.J., Ladd, J.W., and Worzel, J.L., 1979. Seismic evidence for widespread possible gas hydrate horizons on continental slopes and rises. *AAPG Bull.,* 63:2204–2213.

Suess, E., von Huene, R., and the Leg 112 Shipboard Scientists, 1988. Ocean Drilling Program Leg 112, Peru continental margin, Part 2. Sedimentary history and diagenesis in a coastal upwelling environment. *Geology,* 16:939–943.

Taira, A., Hill, I., Firth, J.V., et al., 1991. *Proc. ODP, Init. Repts.,* 131: College Station, TX (Ocean Drilling Program).

Tamano, T., Toba, T., and Aoki, Y., 1984. Development of fore-arc continental margins and their potential for hydrocarbon accumulation. *Proc. World Pet. Cong.,* 11:135–145.

Taylor, M.H., Dillon, W.P., and Pecher, I.A., 2000. Trapping and migration of methane associated with the gas hydrate stability zone at the Blake Ridge Diapir: new insights from seismic data. *Mar. Geol.,* 164:79–89.

Tréhu A.M., Bohrmann, G., Rack, F.R., Torres, M.E., et al., 2003. *Proc. ODP, Init. Repts.,* 204 [CD-ROM]. Available from: Ocean Drilling Program, Texas A&M University, College Station TX 77845-9547, USA.

Figure F1. Bathymetric map showing Nankai Trough study area with ODP Leg 131, 190, and 196 drill sites and outline of the 3-D seismic reflection survey. Contours = water depth in kilometers. Small white line = portion of Inline 284 that passes through Hole 808I, which is shown in Figure **F2,** p. 12. Small yellow line = segment of Inline 284 shown in Figure **F4D** and **F4E,** p. 15. Green line = portion of Inline 215 shown in Figure **F5,** p. 16. Inset shows plate tectonic setting and the Philippine Sea plate vector relative to the Amurian plate.

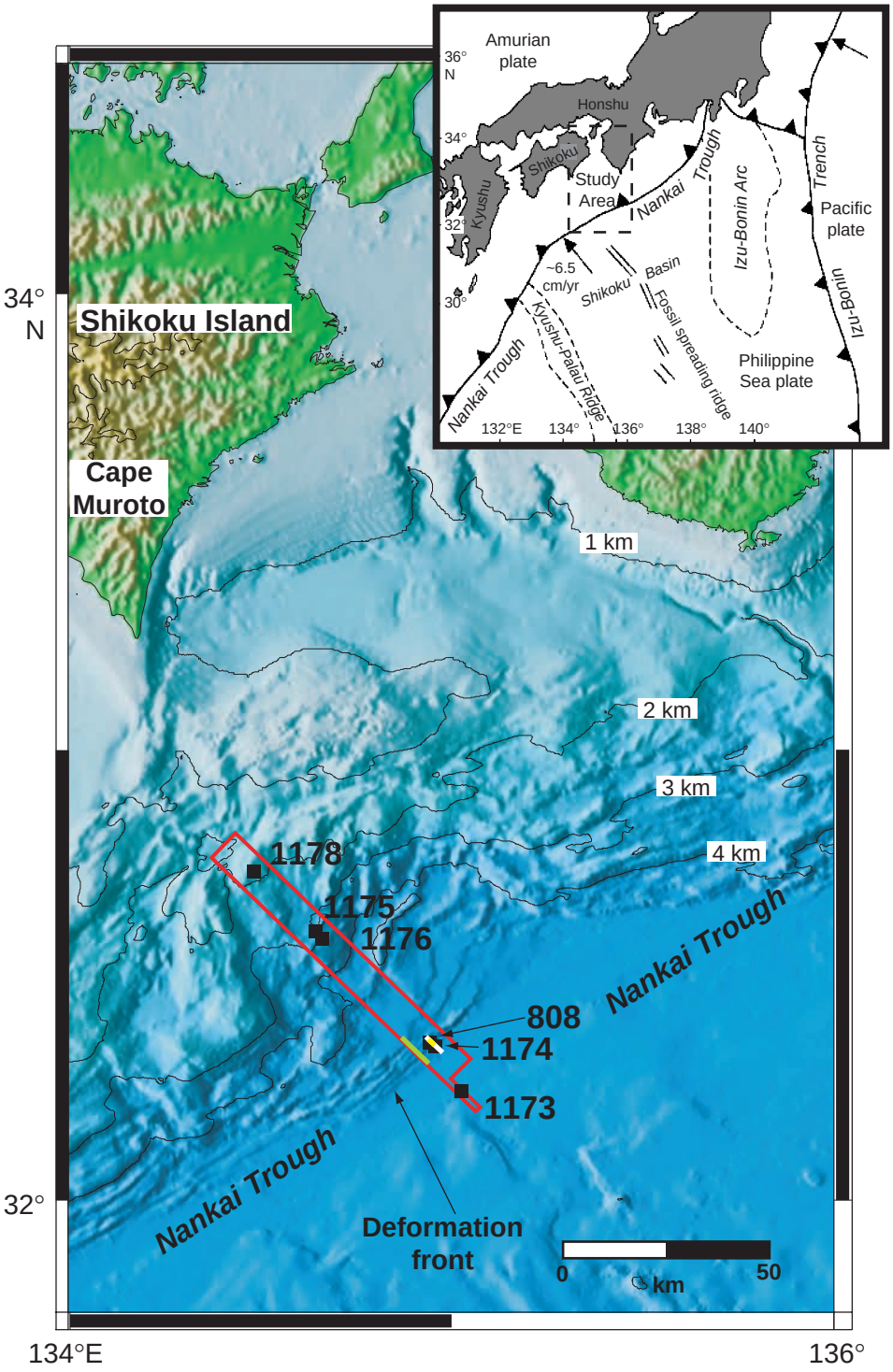

Figure F2. Inline 284 from the 3-D volume that passes through Hole 808I and within 100 m of Hole 1174B (location shown in white in Figure **F1,** p. 11). Color bar shows positive amplitude (yellow to red) and negative amplitude (gray to black) spectrum. Note the lack of a fault-plane reflection along the protothrust fault and the clear negative polarity fault plane reflection from the frontal thrust. Depth is in meters below sea level (mbsl).

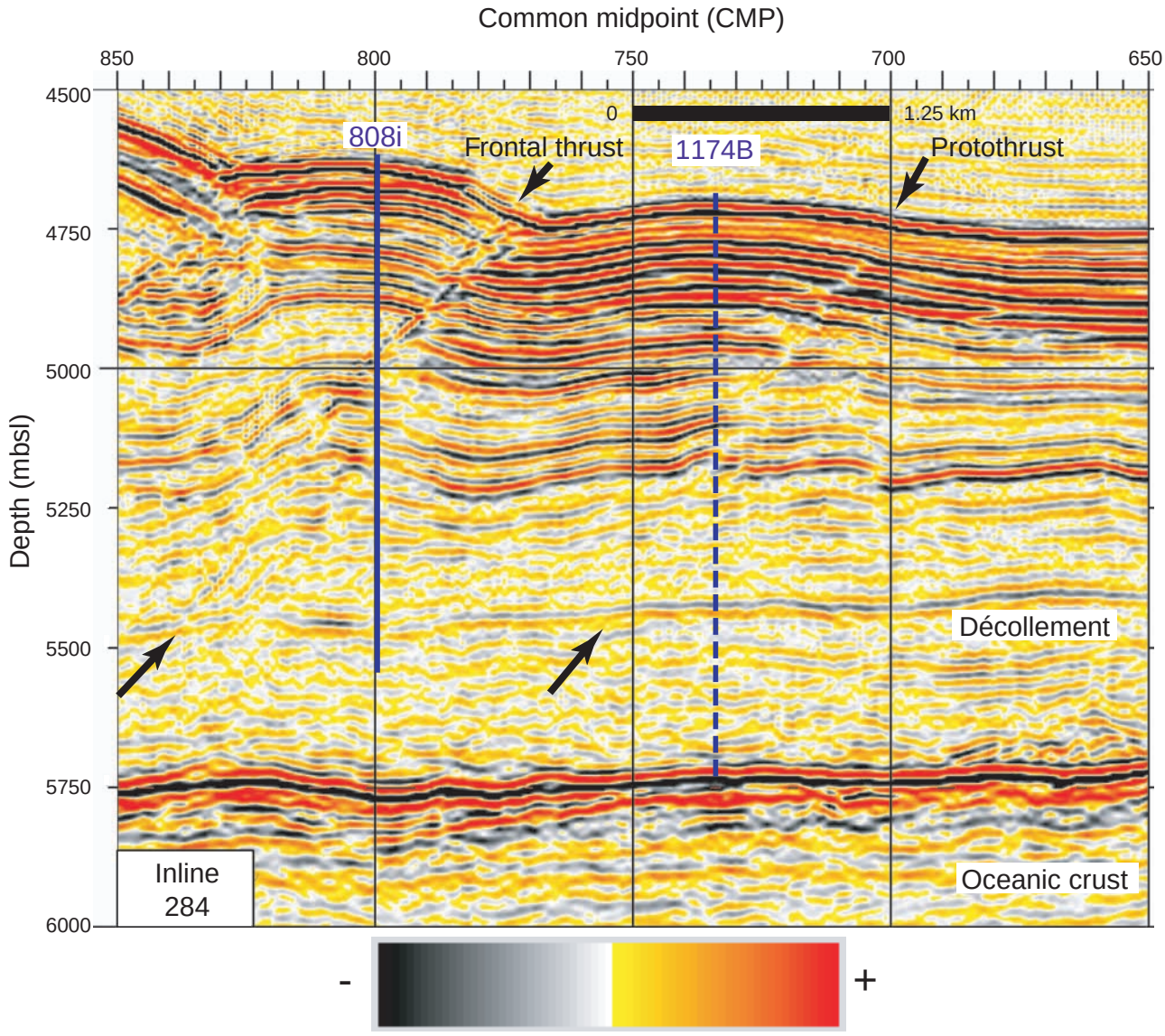

Figure F3. A. 3-D perspective view of the thrust faults that make up the imbricate thrust zone with Inline 360 shown as the backdrop (VE = 2.5X) (structural interpretation presented in Gulick et al., 2004). **B.** Thrust planes from part A are shown flattened into 2-D with amplitudes of the fault plane reflections displayed. Increasing negative polarity is displayed as white to blue shaded pixels (darker blues are more negative), whereas increasing positive polarity is in the red spectrum (darker reds are more positive). Observe the decreasing amplitudes landward of the frontal thrust.

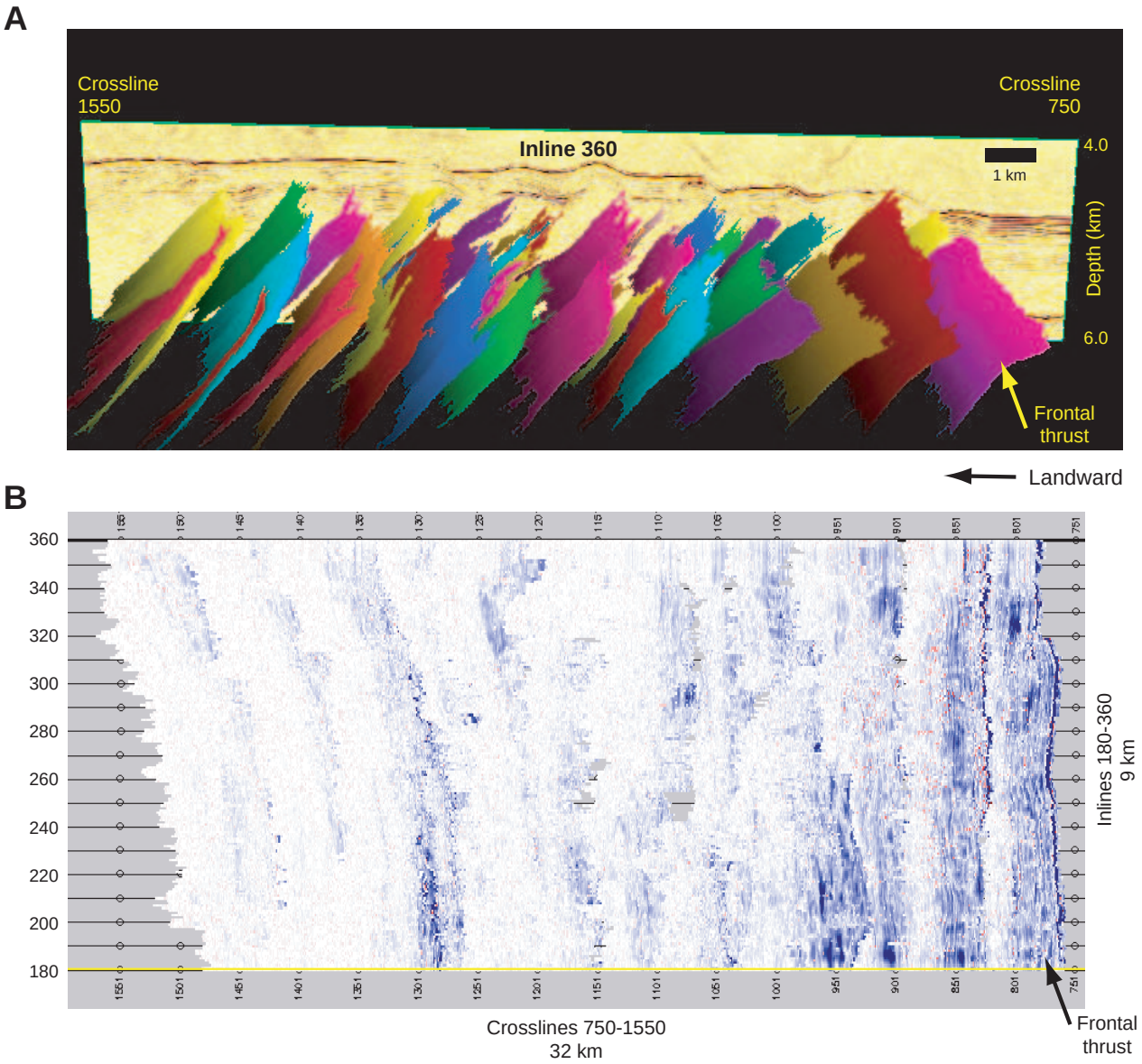

Figure F4. A. Core-derived velocity and density plotted with depth for the 10 m above and below the proto-thrust fault (represented by the dashed line at 550 mbsl) at Hole 1174B showing only a minor velocity decrease near the fault and no clear fault zone. **B.** Logging while drilling (LWD) velocity and density for the frontal thrust fault (center at dashed line at 412 mbsl) at Hole 808I revealing a clear drop in density and velocity across a more developed fault zone. **C.** 1-D model built for 20 m surrounding the frontal thrust (values replaced in the 10 m surrounding fault), in which the frontal thrust is a low velocity and density layer ~1 m thick. (Continued on next page.)

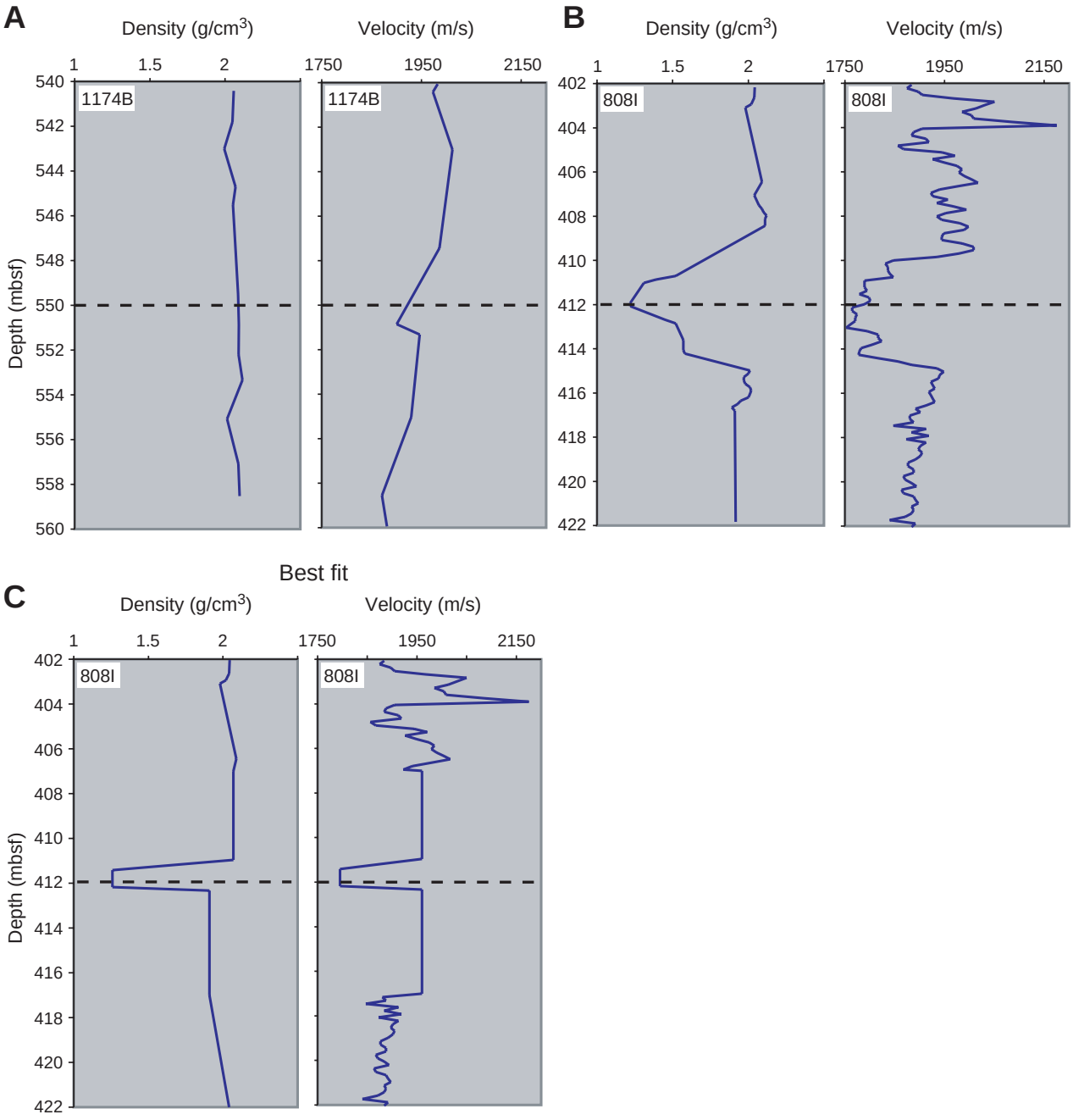

Figure F4 (continued). D. Synthetic built using the LWD velocities and densities overlain over 60 traces of Inline 284 (total width of panel = 1.5 km) centered on Hole 808I. The orientation of the seismic sections in this figure is reversed relative to previous and subsequent figures. Positive peaks are colored red, and negative peaks are colored yellow. Note that the waveform matches well for a 4 m fault zone, but the amplitude is significantly larger. **E.** Synthetic seismogram display over same seismic data as in D, but built using the 1-D model in C. This synthetic seismogram agrees well in amplitude and waveform with the acquired seismic data at Site 808. Depths are in meters below seafloor (mbsf).

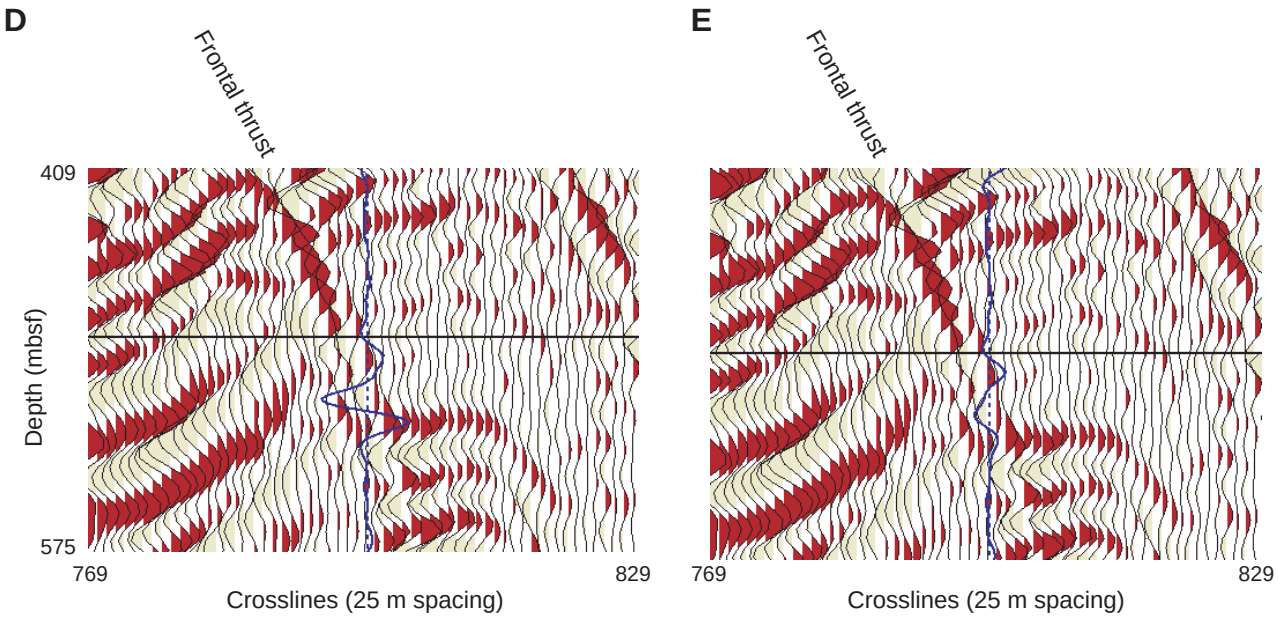

Figure F5. Inline 215 from the 3-D volume that shows an example of the fault-plane reflections brightening with decreasing depth and then ceasing at the bottom-simulating reflector (BSR). This correlation is prevalent throughout the 3-D volume. Color bar shows positive amplitude (yellow to red) and negative amplitude (gray to black) spectrum. Depth is in meters below sealevel (mbsl).